Published in final edited form as:
Acta Biomater. 2011 March ; 7(3): 1249–1264. doi:10.1016/j.actbio.2010.11.007.

Early Osteogenic Signal Expression of Rat Bone Marrow Stromal Cells is Influenced by Both Hydroxyapatite Nanoparticle Content and Initial Cell Seeding Density in Biodegradable Nanocomposite Scaffolds

Kyobum Kim[1], **David Dean**[2], **Anqi Lu**[1], **Antonios G. Mikos**[3], and **John P. Fisher**[4,*]

[1] Dept. of Chemical and Biomolecular Engineering, University of Maryland, College Park, MD

[2] Dept. of Neurological Surgery, Case Western Reserve University, Cleveland, OH

[3] Dept. of Bioengineering, Rice University, Houston, TX

[4] Fischell Dept. of Bioengineering, University of Maryland, College Park, MD

Abstract

Incorporation of hydroxyapatite (HA) within a degradable polymeric scaffold may provide a favorable synthetic microenvironment that more closely mimics natural bone tissue physiology. Both incorporation of HA nanoparticles and alteration of paracrine cell-cell signaling distances may affect the intercellular signaling mechanism and facilitate the enhanced osteogenic signal expressions among the implanted cell population. In this study, we investigate the effect of the incorporation of HA nanoparticles into poly(propylene fumarate) (PPF) scaffolds on the surface properties of composite scaffolds and early osteogenic growth factor gene expression in relation to initial cell seeding density. The result of surface characterization indicated that HA addition improved surface properties of PPF/HA composite scaffolds by showing increased roughness, hydrophilicity, protein adsorption, and initial cell attachment. Rat bone marrow stromal cells (BMSCs), which were CD34(−), CD45(−), CD29(+), and CD90(+), were cultured on 3D macroporous PPF/HA scaffolds with two different initial cell seeding densities (0.33 and 1.00 million cells per scaffold) for 8 days. Results demonstrated that endogenous osteogenic signal expression profiles, including bone morphogenetic protein-2, fibroblast growth factor-2, and transforming growth factor-β1, as well as the transcriptional factor Runx2 were affected by both HA amount and initial cell seeding density. Upregulated expression of osteogenic growth factor genes was related to subsequent osteoblastic differentiation of rat BMSCs on 3D scaffolds, as characterized by alkaline phosphatase activity, osteocalcin mRNA expression, and calcium deposition. Thus PPF/HA composite scaffold construction parameters, including incorporated HA amount and initial cell seeding density, may be utilized to induce the osteoblastic differentiation of transplanted rat BMSCs.

[*]Corresponding Author: John P. Fisher, Ph.D., Fischell Department of Bioengineering, University of Maryland, 3238 Jeong H. Kim Engineering Building, College Park, Maryland 20742, w: 301 405 7475, f: 301 405 0523, e: jpfisher@umd.edu, web: http://www.glue.umd.edu/~jpfisher.

Keywords

osteogenic signaling; hydroxyapatite; BMP-2; RT-PCR; bone marrow stromal cells; poly(propylene fumarate)

Introduction

Calcium phosphate bioceramics, such as hydroxyapatite (HA) and tricalcium phosphate (TCP), are promising materials for bone tissue engineered composites due to their mineral composition reflecting native bone tissue both chemically and structurally, with the latter being in regards to their nano-scale features. HA is especially known to possess biocompatibility and it induces an in vitro osteoblastic differentiation of precursor cells as well as enhances in vivo bone formation [1,2]. However, 3D scaffolds fabricated with only HA or other ceramic materials often exhibit brittleness, difficult manufacturing, and slow degradation rates. Therefore, incorporation of HA within a degradable polymeric network may provide a more favorable synthetic microenvironment to more closely mimic natural tissue physiology with the additional properties of a higher mechanical strength. Since fabrication of HA/biopolymer composites could take advantages of the properties of both the components, there have been many studies utilizing the incorporation of HA with various synthetic polymers including poly(D,L-lactic acid-co-glycolic acid) (PLGA) [3–5], poly(L-lactic acid) (PLLA) [6], poly(propylene fumarate) (PPF) [7,8], poly(caprolactone) (PCL) [9], a copolymer [10], and a cyclic acetal hydrogel [11,12].

Nanoscale features of HA particles exhibit more advantageous cellular responses when compared to microsized HA particles. For example, HA nanoparticles coated on glasses demonstrated higher MG-63 cell attachment and proliferation than microsized HA particles due to higher surface area for cell adhesion and lower crystalinity [13]. Similarly, HA nanoparticles embedded in 3D PCL scaffolds have shown enhanced levels of attachment, proliferation, alkaline phosphatase activity, and calcium deposition (i.e., mineralization) of mesenchymal stem cells (MSC) [9]. Therefore, the size of HA particles can affect cell response, particularly attachment, proliferation, and maturation. If nanocomposite materials produced favorable conditions for tissue formation, they could be a candidate material to improve the surface properties of bone tissue substitutes.

Poly(propylene fumarate) (PPF) offers a variety of advantageous properties as a bone substitute material including degradability in physiological environments and suitable mechanical strength. Crosslinked PPF networks can be fabricated via ultraviolet (UV) radiation with the aid of a photoinitiator such as bis(2,4,6-trimethylbenzoyl) phenylphosphine oxide (BAPO) [14]. This photoinitiation technique for crosslinking allows PPF to be used as a resin material for stereolithography, other additive manufacturing strategies, or even as a translucent mold [15–17]. PPF composite scaffolds incorporating nanosized materials such as alumoxane [18–21], carbon nanotubes [22], and β-TCP [23,24] have exhibited improved mechanical properties, enhanced cell attachment, and increased osteoconductivity in an in vivo model. Moreover, PPF/HA composite materials have also shown the superior cell/tissue responses. Specifically, HA incorporation has been observed to improve MC3TC cell proliferation on 2D PPF composite disks over a 7 day period of in vitro culture [7]. In an in vivo study using rat tibia metaphysic implantation, 3D composite scaffolds with PPF and HA particles with 40 nm in diameter showed a faster rate of new bone formation in tibial defect sites than PPF/microsized HA scaffolds, resulting in superior osseointegration [8]. It has been shown that HA would enhance the osteogenic gene expression when it was incorporated with another polymeric scaffold [25]. Therefore, the

present study focused on the effect of HA in PPF composite scaffolds on the endogenous gene expression as well as the subsequent differentiation of a seeded cell population.

Heterogeneous bone marrow stromal cell (BMSC) populations may contain mesenchymal stem cells. Lineage specific differentiation of BMSCs on synthetic scaffolds depends upon effective induction of particular signal molecules such as growth factors, hormones, and cytokines, associated with the desired lineage. One of the crucial factors facilitating osteogenic signal expressions may be cell-to-cell distance, which potentially alters paracrine signaling mechanisms. Another factor may be scaffold construction parameters such as 3D geometry or surface properties. In our previous study, the initial cell seeding density of 2D PPF disks was found to be a factor contributing to the enhancement of requisite osteogenic signal expression of implanted heterogeneous cell populations [14]. In addition to the surface modification of 3D PPF scaffolds through the addition of HA nanoparticles, changing the cell-cell signaling distance by varying the cell seeding density may similarly affect the cellular responses within 3D porous environments. There have been many studies describing the effects of cell seeding density on osteoblastic differentiation in 3D scaffolds, and it has been observed that an optimal cell seeding density in a 3D environment may enhance this response and thus promote tissue regeneration [26–29].

Moreover, controlling construction parameters to optimize engineered bone substitutes could affect various cellular functions such as attachment, migration, proliferation and differentiation. In order to achieve the optimized properties of 3D scaffolds inducing host cell integration, we fabricated 3D macroporous composite scaffolds with PPF/HA nanoparticles by porogen leaching techniques and a photocrosslinking reaction. Using these scaffolds, we investigated how both the surface properties altered by HA nanoparticle incorporation and the intercellular signaling distance changed in relation to cell seeding density. The global hypothesis in this study is that optimizing the construct parameters of 3D composite scaffold may facilitate enhanced expression of osteogenic growth factor genes among the seeded population, where both incorporation of HA nanoparticle and alteration of paracrine cell-cell signaling distance could be controlling factors. The specific objectives of this study were: (1) fabricate and characterize the physical properties of the 3D macroporous PPF/HA scaffolds, (2) to investigate the effect of HA content and initial cell seeding densities on the stimulated endogenous expression of osteogenic growth factor genes, and (3) to determine the downstream osteoblastic differentiation of rat BMSCs influenced by the enhanced gene expression levels in 3D macroporous PPF/HA scaffolds.

Materials and Methods

PPF/HA composite scaffold fabrication

PPF was synthesized as described previously [14,30]. PPF with number average molecular weight (Mn) of 1300 g/mol and PDI of 3.7 was used throughout this study. Purified PPF was heated to reduce the viscosity and first mixed with 0.5 wt% of BAPO (Ciba Specialty Chemicals Corp., Tarrytown, NY). For composite disks and scaffold fabrication, HA nanoparticles of average grain size 100 nm with crystal structures (BABI-HAP-N100, Berkeley Advanced Biomaterials, Berkeley, CA) [31] with the ratio of 0, 10, and 20% of PPF:HA were incorporated into the PPF/BAPO mixture. For 2D solid disks, the PPF/BAPO/HA mixture without any porogen was uniformly placed between the glass plate and crosslinked in an ultraviolet (UV) light box (intensity of 2.68 mW/cm^2) for 2 hrs. Crosslinked composite sheets were cut into the disks with 18 mm in diameter and 1.5 mm thickness. For 3D macroporous scaffolds, the PPF/BAPO mixture was homogeneously mixed with a NaCl porogen (180–300 μm, 75 wt %) and HA nanoparticles, respectively. The total mixture was then packed into a glass mold. After 2 hr of UV radiation, the crosslinked PPF/HA cylinders were retrieved by breaking the glass molds and cut into small

disks (6.5 mm in diameter and 3 mm in thickness). The disks were then placed in the water for 72 hr to leach out the NaCl porogen. After salt leaching, the resulting macroporous scaffolds were dried and post-cured in the same UV light box for 2 hr. Both 2D disks and 3D scaffolds were washed in acetone for 3 min to dissolve any unreacted components such as residual DEF or short chains of PPF, and air trapped in the inner pores of the scaffold were removed by creating a vacuum by drawing air from a tube with a syringe. The scaffolds were then washed twice with PBS to remove the residual acetone. Finally, the samples were then either characterized after complete drying or sterilized in 70 % EtOH for cell seeding in subsequent in vitro experiments.

Surface morphology, particle distribution, and atomic composition

A scanning electron microscope (SEM) (SU-70, Hitachi, Tokyo, Japan) was used to examine the morphology of the top surface of the composite substrates and the surface distribution of HA particles on the 2D composite disks after washing steps. SEM images were obtained after precoating of carbon adhesive in secondary electron detection mode at 10 kV acceleration voltage and x1500 magnification. Concurrently, the presence of the HA nanoparticles onto the composite surfaces and their atomic composition were assessed by energy dispersive spectroscopy (EDS) at 10 kV and x800 magnification.

Surface roughness and topography

The surface roughness and topography of the 2D disks was examined by an atomic force microscope (AFM) (Asylum Research, Santa Barbara, CA). The topography of the surface (i.e., a height image) was captured in a tapping mode with 20 × 20 μm^2 scan size and 1 Hz scan rate. A silicon tip with a spring constant of 48 N/m was used for all scans. The height images were flattened with a zero order polynomial function and converted to 3D images. The root mean square (RMS) roughness was calculated from processed images. This test was completed with four replicates in each experimental group (n=4).

3D PPF/HA composite scaffold characterization

For 3D porous scaffolds, weight % porosity was determined based on leached porogen amount. Volume% porosity was evaluated by void volume percent per total volume of a scaffold. It was assumed that this void volume was same as the porogen volume in a scaffold. The porogen volume was calculated from the weight of leached salt porogen and the density of salt. The matrix volume was calculated from the dried scaffold weight after leaching and the density of each formulation of PPF/HA composite. Therefore, the total volume was a sum of porogen volume and matrix volume in this evaluation. Top surface, cross-section, and particle distribution onto the surface were observed by SEM. HA distribution over the 3D macroporous scaffold was qualitatively determined by the simple trypan blue staining as previously described [32,33]. Briefly, scaffolds were soaked in a 0.4 (w/v) trypan blue for 10 sec with vigorous shaking. After washing the samples twice with diH_20, each scaffold was placed in 100% EtOH for 1 min and sonicated for 5 sec to remove any unbound dye. A top surface image of uniformly stained scaffolds depicting the distribution of HA within each composite scaffold was acquired. The level of adsorbed protein onto the scaffold surface was measured by a previously described method [34]. Briefly, the scaffolds were first completely wetted by a series of pre-soaking: 1hr in ethanol, 2 × 30 min in PBS, and overnight incubation in PBS. Samples were then placed in culture media with 10% FBS for 4 hr at 37°C on a shaker table (25 rpm). After incubation, samples were washed with PBS three times, and adsorbed proteins were extracted during two cycles of 1 hr incubation in 250 μl of 1% sodium dodecyl sulfate solution. A BCA protein assay kit (Pierce, Rockford, IL) was used to determine protein concentration. This test was completed with triplicate samples and triplicate measurements.

Mechanical testing

Compressive mechanical testing was conducted according to the American Society of Testing Materials Standard D695-2a using an Instron mechanical tester (Instron 5565, Norwood, MA). Scaffolds with the PPF:HA ratios of 0, 5, 10, 15, and 20% were prepared as cylinders with 13 mm in height and 6.5 mm in diameter. Samples were compressed along their vertical axis at a speed of 1.3 mm/min until the compressive strain reached 0.5 mm/mm. The Young's modulus and yield compressive stress at 1% offset were calculated using Bluehill 2.16 software (Instron). This test was completed with five replicates in each experimental group.

Rat bone marrow stromal cell isolation

Rat BMSCs were isolated from the femurs and tibias of young male Wistar Hanover rats (101–125 g, Taconic) following a University of Maryland approved IACUC animal protocol (R-07-94) according to methods previously described [14].

2D attachment of rat BMSCs

2D PPF/HA composite disks were pre-washed after acetone etching prior to cell seeding in the following manner. Each disk was sterilized with 70% EtOH for 30 min and washed twice with PBS buffer. Then, the disks were soaked in FBS overnight to increase the level of adsorbed serum protein on the composite surfaces. Each disk was then placed in a 12 well plate and an autoclaved stainless steel ring (inner diameter: 16 mm) was also placed onto each disk to confine the seeding area as well as prevent floating of disks [14]. Rat BMSCs in culture flasks that had undergone 3 passages were trypsinized, resuspended in osteogenic (OS) media (Control media contained α-MEM, 10% penicillin/streptomycin antibiotics, and 0.2 mM of ascorbic acid while OS media was made of control media supplemented with 10 mM Na-β-glycerophophate and 10^{-8} M dexamethasone) with 10% FBS, and seeded onto composite disks (60,000 cells per disk, 30,000 cells/cm^2). After 24 hr incubation, the cells on the disks were washed with PBS and stained with 2 μM calcein acetoxymethylester (Calcein AM, Invitrogen) for 30 min at room temperature. Images were obtained using a fluorescence microscope (Axiovert 40 CFL with filter set 23, Zeiss, Thornwood, Swiss) equipped with a digital camera (Diagnostic instruments 11.2 Color Mosaic, Sterling Heights, MI) from five spots (i.e., one in the center and four along each major axis) to quantify the total number of attached cells. A total of 20 images (four biological replicates) were acquired and transferred to Matlab software (The MathWorks, Natick, MA) and converted to black and white binary images. The total number of attached cells in each group was determined.

3D cell culture

3D PPF/HA composite scaffolds were also pre-washed, as described above, before cell seeding. PPF/HA scaffolds were sterilized in 70 % EtOH and soaked in FBS, and then the cells were seeded onto the scaffold. One million cells per scaffold were seeded for the visualization assays while scaffolds with two different cell densities (0.33 million and 1 million cells in 25 μl of cell suspension per scaffold) were tested for alkaline phosphatase (ALP) expression, mineralization, and quantitative real time polymerase chain reaction (qRT-PCR) experiments (see the experimental groups in Table 1). The OS media was changed every 2 days until day 8 and samples were cultured in a static condition.

Visualization of cells on 3D scaffolds

Cell viability was assessed up to day 8 following cell seeding on 3D PPF/HA scaffolds by using Calcein AM fluorescent staining. The cell culture media was removed and the cell/scaffold constructs were rinsed twice with PBS. Staining and microscopic procedures were

performed as described previously. Cell spreading on composite scaffolds was indirectly determined by F-actin staining. After the aspiration of media from each well, each scaffold was washed with PBS, fixed with 500 μl of 4% paraformaldehyde for 30 min, washed three times with PBS, and then incubated in 500μl of 0.2% Triton X-100 in PBS for 2 min. Samples were then washed twice with PBS again, and incubated in 700 μl of diluted (1:40) phalloidin (Alexa Fluor 488, Invitrogen) for 1 hr at room temperature. Stained cytoskeletons were observed under a fluorescence microscope. Cell morphology on the composite surfaces was also examined by SEM. After cell culture media removal, each scaffold was washed with PBS, fixed with 500 μl of 4% paraformaldehyde for 30 minutes, and washed again with PBS three times. Samples were air-dried over night, coated using a gold sputter, and observed via SEM. All three assays were performed on day 1 and 8.

Quantitative reverse transcription polymerase chain reaction (qRT-PCR)

Total RNA was isolated from cell/scaffold constructs using Trizol (Sigma-Aldrich) according to the manufacturer's protocol. cDNA was prepared from the isolated RNA using a High Capacity cDNA Archive kit (Applied Biosystems, Foster City, CA). Pre-amplification of cDNA was performed by the manufacturer's protocol. Briefly, the cDNA sample was mixed with 0.2X pooled Taqman Gene Expression assay mixture (Applied Biosystems) of genes of interest, and a PreAmp Master Mix (Applied Biosystems). The genes of interest included three growth factors (bone morphogenetic protein-2 (BMP-2, Taqman Assay ID: Rn00567818_m1), fibroblast growth factors-2 (FGF-2, Rn00570809_m1), and transforming growth factor-β1 (TGF-β1, Rn00572010_m1)), one transcriptional factor of Runx2 (Rn01512296_m1), and one osteoblastic differentiation marker of osteocalcin (OC, Rn00566386_g1). The thermal condition for the pre-amplification reaction was 10 min at 95°C, and 10 cycles of 15 sec at 95°C and 4 min at 60°C. This pre-amplified cDNA sample was diluted with 1x TE buffer (1:5) and then was utilized to investigate the relative gene expression level of target genes. A house-keeping gene, glyceraldehyde-3-phosphate dehydrogenase (GAPDH, Rn99999916_s1) was used as an endogenous control gene. qRT-PCR was conducted on an ABI Prism 7000 sequence detector (Applied Biosystems), using a thermal condition of 2 min at 50°C, 10 min at 95°C, and 50 cycles of 15 sec at 95°C and 1 min at 60°C. The relative gene expression level of the genes of interest was normalized using the GAPDH control gene. The mean of fold changes compared to the calibrator group (0 Low Group at day 1) was analyzed using a ΔΔCt method and its standard deviation is reported (n=3).

Alkaline phosphatase assay

ALP activity was determined using p-nitrophenyl phosphate (pNPP) enzymatic assay (Sigma-Aldrich, St. Louis, MO) based on the hydrolysis of pNPP to para-nitrophenol, where spectroscopic data of the final yellow product indicates ALP activity. The cell/scaffold constructs were washed with PBS and placed in 600 μl of autoclaved distilled water. Protein and DNA were extracted through three cycles of cell-lysis: freeze (30 min at −80°C), thaw (30 min at 37°C), and sonication (30min, 40 kHz) based on the previous protocol [35]. The resulting debris was centrifuged at 12,000 g for 10 min and the supernatant was transferred to a new sterile tube. The supernatant was mixed with a pNPP liquid substrate and after 1 hr incubation at 37°C in the dark, 2 M NaOH solution was added to stop the reaction. The absorbance was recorded at 405 nm using a M5 SpectraMax microplate reader (Molecular Devices, Sunnyvale, CA). The DNA amount was also quantified using a PicoGreen assay kit (Invitrogen) and the ALP activity level was normalized to the DNA amount and the mM ALP/μg DNA was reported. Each experimental group was analyzed in triplicate.

Mineralization assay

Calcium mineralization was measured by selective binding of alizarin Red S (ARS, Sigma-Aldrich) to calcium salts. On day 8 and 15, cell/scaffold constructs were washed with PBS, fixed with 4% paraformaldehyde for 30 min at room temperature, and then stained with 40 mM ARS/PBS solution (pH 4.1) on the shaker (150 rpm) for 30 min at room temperature. After washing five times with dH_2O to remove any unbound ARS, 10 v/v% acetic acid was applied to each sample to dissolve the crystals. Optical density was recorded at 405 nm using a microplate reader and the background intensity of a control scaffold (i.e., a scaffold without cells) was subtracted from each sample. The calcium amount was normalized to the DNA amount and mM ARS/μg DNA was reported. Each experimental group was analyzed in triplicate.

Statistical analysis

The data from all studies were analyzed by an analysis of variance (ANOVA) and Tukey's multiple-comparison test. A p value < 0.05 was utilized to demonstrate significant difference between the experimental groups. The means and the standard deviations were reported in each figure.

Results

2D surface characterization

The PPF/HA composite material was fabricated through a simple physical mixing technique and a crosslinked PPF network was obtained by UV light photoinitiation. The surface morphology was observed by SEM imaging and the atomic composition as well as calcium (Ca)/phosphate (P) ratio of the composite was analyzed by EDS analysis (Point of interest). In addition, the surface topography and RMS roughness were assessed by AFM. Increasing the amount of HA nanoparticles incorporated within a PPF polymer network resulted in more particles being exposed on the composites material's surface (Figure 1A, 1C, and 1E). Based on the EDS analysis data, it should be noted that Ca/P ratio of exposed HA particles on the composite surface was consistent regardless of incorporated HA amount. The Ca/P ratio was 1.92 ± 0.21 in PPF/HA 10% group and 1.98 ± 0.12 in PPF/HA 20% group (Table 2). This ratio is similar to that of initial HA particles without any processing (i.e., 67.2:32.7) [12]. This observation confirms the stoichiometry of HA was consistent during the fabrication steps presented in this study. HA incorporation also resulted in increasing surface roughness (Figure 1B, 1D, and 1F). 3D height images using AFM also qualitatively demonstrated that a rougher surface was obtained by mixing larger amounts of HA particles into the PPF. RMS roughness data in Figure 1G shows a significant increase in roughness after acetone etching in the PPF/HA 10% and 20% groups compared to the PPF control group ($p = 2.96\times10^{-6}$). Moreover, these two groups also shows a significant increase in roughness when simply etched by acetone compared with non-etched samples ($p = 4.79\times10^{-4}$ and 3.18×10^{-5}, respectively) implying that some portion of the embedded HA particles in PPF were exposed by acetone washing and resulted in a rougher surface than in either the PPF control or the non-treated PPF/HA samples. Therefore, the PPF/HA composite fabrication techniques by physical mixing, photocrosslinking reaction, and acetone etching are suitable to create higher surface roughness with a different chemical composition. This observation in 2D PPF/HA disks could be contributed to the characteristics of a surface of 3D porous PPF/HA scaffolds.

3D scaffold characterization

SEM analysis was also performed on the structure of 3D macroporous PPF/HA scaffolds (Figure 2). Top surface (Figure 2A) and cross-section (Figure 2B) images demonstrated

highly interconnected 3D porous structures. The weight % porosity measured by the amount of salt leached demonstrated that all three experimental groups showed over 75 wt% of leaching (n=6), implying that the pores in the scaffold are interconnected which would allow water to flow through the inner structure while calculated volume % porosity was slightly increased as HA amount increased. For the higher magnification of the surface of 3D PPF/HA scaffolds, the same trends associated with HA particle distribution were observed, as were seen on the 2D disks (Figure 2C). This suggests that a simple porogen leaching technique could be applied to fabricate well-interconnected 3D PPF/HA scaffolds with high porosity. For the mechanical testing, the PPF/HA 20% group showed a significantly higher modulus than either the PPF control or the PPF/HA 10% group ($p = 1.05\times10^{-2}$) (Figure 3A). The offset yield strength in PPF/HA 20% was also higher than in the other groups (Figure 3B). In addition, the adsorption of hydrophilic trypan blue dye to the composite scaffolds qualitatively demonstrated the uniform distribution of the HA particles onto the surfaces, increasing hydrophilic nature of the composite surfaces, and subsequently increasing potential to adsorb dye by increasing the amount of incorporated HA (Figure 4) although the aggregation of HA particles was somehow observed. The hydrophobic PPF control (Figure 4A) did not adsorb trypan blue while more dye was adsorbed in the PPF/HA 10% and 20% groups (Figure 4B and 4C). Similarly, the amount of protein adsorbed to the surface of the 3D scaffolds increased with the addition of more HA particles (Figure 4D). The PPF/HA 20% group showed a significantly higher protein adsorption compared to the PPF control group ($p = 3.76\times10^{-3}$). This result suggests that a higher level of HA incorporation resulted in increasing surface roughness and that a higher concentration of HA exposed on the surface might elevate the hydrophilicity and subsequent protein adsorption level. Along with the improved physical characteristics with increasing the amount of HA, the mechanical properties such as Young's modulus and yield strength of the 3D structures were also increased.

Cell attachment

As measured by fluorescently stained cell-area, the qualitative images of Calcein AM staining in Figure 5A reveals that more cells are attached to the composite scaffolds as HA concentration increases. For quantification, the total cell-attached area in each group was normalized by that of the TCPS control. The percent attachment in the PPF/HA 20% group was significantly higher than the other groups ($p = 2.05\times10^{-4}$). Rat BMSC attachment was increased with increasing surface roughness which in turn depended on HA particle concentration in these composite scaffolds. These results demonstrated that increased HA particle incorporation in PPF scaffolds increased surface roughness, subsequent protein adsorption from the media to the surface of the composite, and resulted in more cells favorably attaching to the composite scaffold surface.

Viability, cell spreading, and cellular morphology

To characterize rat BMSC viability on 3D porous PPF/HA scaffolds, Calcein AM staining was performed (Figure 6A). The cytoskeleton development of cells was examined by F-actin staining (Figure 6B) while cellular morphology was observed by SEM (Figure 6C). Calcein AM staining data demonstrated that the cells in all experimental groups were viable for up to 8 days of in vitro culture in OS-conditioned media. Along with 2D attachment data on day 1 (Figure 5A), PPF and PPF/HA composite materials supported a suitable environment for rat BMSCs in the 3D scaffolds. Images of F-actin staining qualitatively demonstrated that more cells spread in PPF/HA 20% groups than the PPF control group on day 1, however all groups showed similar levels of cell spreading on day 8 (Figure 6B). This result is also correlated with the change of cellular morphology observed by SEM on day 1, where observable cell flattening was seen on the surface of the PPF/HA 20% groups, while some

of cells on control PPF retained a rounded shape (Figure 6C). On day 8, the cells on PPF/HA composite scaffolds were highly flattened and covered the surface of these scaffolds.

Osteogenic signal expression profiles

Quantitative RT-PCR was performed to investigate the effect of HA nanoparticle incorporation with various seeding densities on osteogenic signal expression. For higher seeding density groups, BMP-2 gene expression generally decreased or was stagnant for all HA amount groups (Figure 7A). However, the addition of HA along with high cell seeding density increased BMP-2 expression compared to the PPF control on day 8 ($p = 9.83\times10^{-6}$). This observation was similar to the low cell seeding groups: PPF control group with low cell seeding showed decreasing BMP-2 expression over 8 days while 10 Low and 20 Low groups exhibited significantly higher expression level than PPF control on day 8 ($p = 2.96\times10^{-8}$), and this level was also significantly higher than 10 High and 20 High groups ($p = 4.38\times10^{-5}$ and $p = 1.46\times10^{-5}$, respectively). Increased HA incorporation in the low cell seeding density groups (10 Low and 20 Low) was also observed to be correlated with increased BMP-2 expression after 8 days of culture over the initial expression level on day 1.

FGF-2 expression represents a similar pattern to the TGF-β1 expression profile (Figure 7B and 7C). Among high cell seeding density groups, 20 High exhibited 3 fold up-regulation of FGF-2 on day 4 and kept this level until day 8 ($p = 3.81\times10^{-4}$). Moreover, 10 High also showed a 2.95 fold up-regulated FGF-2 expression on day 8 and both 10 High and 20 High exhibited significantly higher FGF-2 expression than the PPF control group on day 8 ($p = 6.94\times10^{-3}$). A similar up-regulation pattern was also observed in the low cell seeding density groups on day 8: FGF-2 expressions of both 10 Low and 20 Low were significantly higher than 0 Low on day 8 ($p = 1.03\times10^{-8}$) and this level was also up-regulated over the day 1 expression level. Specifically, 20 Low exhibited more than a 4.7 fold change compared to the calibrator group. A general decreasing trend of TGF-β1 expression was also observed in the PPF control groups for both cell seeding density groups over 8 days. For the higher cell seeding density groups, HA addition induced more TGF-β1 expression than in the PPF control, but this level was below than the expression of the calibrator group on day 1. A significant increase of TGF-β1 was found in 20 Low group on day 8 versus 0 Low and 10 Low groups ($p = 1.48\times10^{-2}$), and this up-regulation was more than a 2 fold increase compared to the calibrator group.

The Runx2 transcription factor expression in the high cell seeding density groups showed a decreasing pattern over 8 days except 20 High group, which showed a peak on day 4 (Figure 7D). All groups with low cell seeding density exhibited down-regulation of Runx2 expression on day 4 and an increased expression by day 8.

Osteoblastic differentiation

In order to investigate whether the cell population would differentiate into an osteoblastic lineage by changing the HA amount in the scaffolds, and/or the initial cell seeding density, ALP protein activity was assessed (Figure 8). A correspondence between ALP activity and the HA particle amount was only observed in lower cell seeding density groups on day 1 and a higher cell seeding group (20 High) on day 4, compared to the PPF control group. During the later time points, 0 Low group on day 4 ($p = 8.01\times10^{-4}$) and both 0 Low and 10 Low groups on day 8 ($p = 1.01\times10^{-2}$ and 4.31×10^{-3}, respectively) exhibited significantly higher ALP activity compared to higher cell seeding density groups. Late osteoblastic differentiation was assessed by calcium deposition (Figure 9) and the OC mRNA expression (Figure 10). Increasing HA content in both cell seeding density groups resulted in higher mineralization. On day 8, 20 High group showed significantly higher calcium deposition

than the PPF control group and both 10 and 20 Low groups also showed significantly higher mineral contents ($p = 6.62\times10^{-6}$). On day 15, 20 High group at both cell seeding densities showed significantly increased calcium deposition over the PPF control group ($p = 4.53\times10^{-4}$). Moreover, 10 and 20 Low groups presented a significant increase in mineralization versus the high cell density groups on day 8 while mineralization on day 15 was statistically unchanged when cell seeding density was varied. In Figure 10, it can be seen that the OC mRNA expression in all groups exhibited an increasing trend over 8 days. By day 4, 20 High group exhibited a significantly higher OC expression level than did the other groups. On day 8, the expression level of HA incorporated PPF groups was higher than the PPF control group for both cell seeding densities ($p = 3.08\times10^{-5}$). Although the effect of cell seeding density on OC expression was not observed on day 8, the effect of HA amount on the expression (i.e., increased osteoblastic differentiation with higher HA concentration) was related with calcium deposition, as seen in Figure 9.

Discussion

The main objective of this study was to determine which 3D PPF/HA nanoparticle composite scaffold parameters facilitate endogenous gene expression of osteogenic growth factors contributing osteoblastic differentiation. In order to optimize the construct properties that mimic the native bone healing process, controlling parameters that enhance the expression of signaling molecules such as the physical properties of the scaffold and intercellular signaling distance were characterized. It appears that the incorporation of HA nanoparticles into PPF resulted in an alteration of surface properties of these composite materials including topography, roughness, calcium and phosphate atomic ratio, and ability to absorb proteins. In addition, changing initial cell seeding density altered cell-cell paracrine signaling distance among the transplanted cell population. Therefore, it is of importance to characterize the proper conditions of those parameters that control or at least facilitate the stimulation of specific osteogenic growth factor expression. To this end, we aim to investigate both the effect of the amount of HA incorporated in PPF scaffolds and the initial cell seeding density on endogenous osteogenic growth factor gene expression profiles and osteoblastic differentiation.

We fabricated well-interconnected 3D macroporous PPF/HA scaffolds via simple techniques using porogen leaching and photocrosslinking. The characterization data in Figure 1 demonstrates that HA nanoparticle incorporation resulted in uniform distribution of HA and higher level of calcium and phosphate on the surface of composites. Moreover, HA incorporated composite scaffolds exhibited rougher surface topography as confirmed by RMS roughness data. Subsequently, surface properties modified by HA nanoparticle incorporation also resulted in higher levels of passive protein adsorption onto the scaffold surface perhaps due to increasing higher hydrophilicity (i.e., wettability) of scaffolds qualitatively measured by hydrophilic dye adsorption (Figure 4). Both of these factors may improve initial cell attachment since higher roughness provides more surface area with more complex geometry for cells to attach to, and increasing hydrophilicity is directly related with the adsorption of proteins existing in the aqueous media [9]. This present study also verified this relation by showing that higher rat BMSC attachment was observed in PPF/HA 20% composite than in control PPF samples in a 2D environment (Figure 6). In addition, qualitative visualization of cells on 3D PPF/HA composite scaffolds also demonstrated more cytoskeleton development on PPF/HA 20% scaffolds than on PPF control scaffolds on day 1 as assessed by F-actin staining (Figure 7(B)). The SEM images also qualitatively demonstrated morphological changes in cell flattening with more cell flattening observed as HA incorporation in composite scaffolds was increased (Figure 7(C)). This result may be explained by HA nanoparticles potentially playing a functional role in the integrin-mediated cell adhesion. Generally, initial cell adhesion to extracellular matrix (ECM) is mediated by

an integrin transmembrane receptor [36]. Integrin binding to ECM proteins physically connects the cell's cytoskeleton and the surrounding ECM. This initiates the intracellular signaling pathway to nucleate the signaling proteins such as focal adhesion kinase. For example, controlled HA deposition has been observed to induce MC3T3-E1 cell adhesion, integrin presentation and clustering, and focal adhesion complex mediation[37]. Since the integrin binding and initial cell attachment play a critical role in downstream signaling cascades such as the interaction of cytoskeleton protein/cellular membrane protein/ECM proteins, induction of signal transduction, stimulation of transcription factors, and consequent gene expression [38,39], HA nanoparticle incorporation may stimulate not only initial cell adhesion but also osteogenic growth factor gene expressions during osteoblastic differentiation.

The compressive Young's modulus and off-set yield strength of PPF/HA composite scaffolds were determined in order to investigate scaffold's load-bearing capacity and its potential as a bone substitute (Figure 3). The compressive modulus of the 3D PPF/HA composite scaffolds exhibited similar levels to that of native human cancellous bone (i.e., 2 to 10 MPa) [40]. The PPF/HA 20% group exhibited significantly higher Young's modulus than the PPF control and PPF/HA 10% groups. Composite scaffolds presented a trend of increasing Young's modulus relative to HA nanoparticle reinforcement, and this has been observed in other studies. For example, polycarbonate/HA nanoparticle composite scaffolds exhibited an increase of Young's modulus from 0.6 GPa to 4.5 GPa when the amount of HA was increased from 10% to 30% [41]. Similarly, PLG/HA composite also showed an increase in Young's modulus when the ratio of PLG:HA was increased up to 1:5 [32]. One possible explanation of observed mechanical enhancement could be the intrinsic contribution of HA as well as an increase in surface to volume ratio with HA nanoparticle addition, which also found in PCL/HA composites [42,43]. Therefore, the mechanical properties of photocrosslinked porous PPF/HA nanocomposite scaffolds observed in this study demonstrated that these properties can be controlled during fabrication, a possibly useful fact for manufacturing bone tissue engineering scaffolds.

The effect of HA amount on endogenous osteogenic gene expression in composite scaffolds with varying cell seeding density was investigated. There have been many studies about the effect of exogenous growth factors on osteoblastic differentiation; however, the present research has shown for the first time the effect of HA presence on endogenous osteogenic gene expression including BMP-2, FGF-2, TGF-β1, and Runx2. BMP-2 is known to participate in the regulation of cell growth and differentiation along with the induction of osteogenic progenitor cells in bone defect sites during the healing process. Although there have been many studies on exogenous BMP-2 administration to culture media as well as delivery of this growth factor to the healing defect site, the present study demonstrated that endogenous osteogenic signal expressions could be facilitated by altering scaffold construction properties of cell/scaffold integration through the incorporation of HA nanoparticles and changing the initial cell seeding density. Despite of the fact that BMP-2 gene expression level was decreased or was unchanging for PPF control scaffolds, the HA incorporated composite scaffolds induced significantly higher BMP-2 expression than the control on day 8 ($p = 9.83\times10^{-6}$ in high cell seeding and 2.96×10^{-8} in low cell seeding). This HA-induced BMP-2 upregulation was observed for both cell seeding densities (Figure 8(A)). The upregulated level of BMP-2 expression was higher in the lower cell seeding density on day 8. Therefore, it seems that PPF/HA composite scaffolds may stimulate higher endogenous BMP-2 expression and its expression level may be also be responsive to the initial cell seeding density.

We have previously speculated on the interaction of endogenous signal expression with other signaling factors of rat BMSCs cultured on 2D PPF disks previously [14]. BMP-2

signaling is dependent on the expression of Runx2 transcription factor through the Smad and MAPK intracellular signaling pathways [44,45], and our comparison with BMP-2 and Runx2 expression profiles in this study might confirm this interaction. Early decline of BMP-2 in all groups except the 20 High group in a 3D scaffold by day 4 was also associated with Runx2 deactivation as seen in Figure 8(D). Specifically, an increase in BMP-2 expression in the 20 High group by day 4 might be related to increasing Runx2 expression by day 4. For later time points, from day 4 to 8, the high cell seeding density groups exhibited a general decline of BMP-2 expression although HA incorporation resulted in different levels of expression on day 8 and Runx2 expression profile in high cell seeding groups showed the same decreasing pattern by day 8. During this period, low cell seeding groups exhibited increasing BMP-2 expression that might be also related to an increase in Runx2 expression in all HA incorporated groups. In addition, FGF-2 expression (Figure 8(B)) was also exhibited Runx2-mediated endogenous gene expression. FGF-2 expression could be stimulated by Runx2 induction via MAPK pathway [46]. The result in low cell seeding density (0.33 million cells/scaffold in this study) showed a decreased FGF-2 expression by day 4 and an increased level by day 8. This expression profile might be related to BMP-2 and Runx2 expression pattern described early. However, a discrepancy in the high cell seeding density groups (1 million cells/scaffold) was observed, which is that up-regulation of FGF-2 expression in 10 and 20 High groups during the later time points was not related to the down-regulation of Runx2 in the same groups. This might be explained by the possibility that Runx2 stimulation was more affected by BMP-2 stimulation via both the Smad and MAPK pathways, rather than FGF-2 expression through the MAPK pathway only. Therefore, the decline of BMP-2 in high cell seeding groups on day 8 might relate with Runx2 down-regulation, even in the presence of FGF-2 up-regulation. Moreover, since the expression levels of BMP-2, FGF-2, and TGF-β1 in lower cell seeding density on day 8 were higher than those in lower cell seeding density, it is also suggested that 0.33 million cells/scaffold in this study might be a more favorable condition to facilitate the osteogenic gene expressions in PPF/HA composite scaffolds.

FGF-2 is associated with the stimulation of osteoblasts through the Cbfa-1/Runx2 transcription factor activation [47] as well as angiogenic development [48]. Therefore it is imperative to investigate its signaling profiles to promote the integration of implanted scaffolds with surrounding host tissues for bone tissue regeneration. In the FGF-2 expression profile in Figure 8(B), it was observed that its expression increased at a later time point of day 8 and that the HA addition in composite scaffolds may have facilitated statistically higher FGF-2 expression that was not observed in the PPF control group. The PPF/HA 10% and 20% groups exhibited higher FGF-2 expression level than did the PPF control on day 8 for both cell seeding densities. In particular, 20% HA nanoparticle addition to composite with 0.33 million cell seeding showed up to a 5 fold change by day 8. This observation of upregulated osteogenic signal expression with HA nanoparticle incorporation was related to BMP-2 expression and could be evidence of an effect on osteogenic signal expression by altering scaffold construction properties. The results in Figure 8(C) also demonstrated that HA incorporation into composite scaffolds at both cell seeding densities enhanced the TGF-β1 expression on day 8 from both cell seeding densities, as was the case with FGF-2 expression. Our previous study demonstrated that the existence of optimal cell seeding density of transplanted rat BMSC populations on 2D PPF disks appeared to facilitate BMP-2, FGF-2, and TGF-β1 expression [14]. This present study using 3D PPF/HA porous scaffolds also demonstrated that the optimum condition to induce more osteogenic signal expression was the PPF/HA 20% group with 0.33 million cells.

The effect of HA nanoparticle contents on the osteoblastic differentiation of rat BMSCs was investigated with two different cell seeding densities. ALP protein expression was examined as a transient early osteoblastic differentiation marker, while calcium deposition and OC

mRNA expression was assessed as an indicator of a later stage of differentiation. The ALP expression level depended on the amount of HA nanoparticles incorporated into the scaffolds. This was a statistically significant parameter in lower cell seeding density groups on day 8 (Figure 9). In addition, the results also demonstrated that mineralization and OC mRNA expression also depended on HA addition to the scaffolds (Figure 10 and 11). Both HA incorporated composite scaffolds exhibited significantly higher calcium deposition with both cell seeding densities on day 8 ($p = 6.50\times10^{-4}$ in high cell seeding and 1.48×10^{-3} in low cell seeding) and the effect of HA amount on mineralization was greater in the lower cell seeding density groups. The PPF/HA 20% groups showed higher levels of mineralization for both cell seeding densities on day 15. Similarly, the OC mRNA expression data also showed the dependence of late osteoblastic differentiation of BMSCs on the amount of HA present. Significantly higher OC expression was observed when HA concentration increased on day 8 even though an effect of cell seeding densities was not observed. The potential dependence of osteoblastic differentiation on incorporated HA amount is in agreement with several other studies. One of these recent studies showed that the incorporation of 50 ng of HA nanoparticles into cyclic acetal hydrogels stimulated more endogenous ALP mRNA expression of encapsulated rat BMSCs than 5 ng and control hydrogel groups on day 8 [12]. In the same study, OC mRNA expression in 5 and 50 ng of HA groups was significantly higher than the control (without HA) on day 1, 4, and 8. Therefore, increasing amount of incorporated HA particle might enhance the osteoblastic differentiation. OC and osteopontin (OP) mRNA expression of rabbit BMSCs in a 2D monolayer has also been observed to be dependent on HA nanoparticle concentration [49]. Moreover, osteoblastic differentiation with HA dependence has also been observed in human MCSCs on PLG/HA composite scaffolds and both ALP and OP protein expression levels were higher by increasing the HA:PLG ratio for up to 28 days [32]. Therefore, our PPF/HA composite scaffold may also facilitate osteoblastic differentiation of transplanted rat BMSCs by increasing the amount of incorporated HA amount and by varying the initial cell seeding density.

Conclusions

This investigation of scaffold construction properties for 3D macroporous PPF/HA scaffolds appears to have found parameters that facilitate osteoblastic differentiation of transplanted cell populations and evidence of associated osteogenic signal gene expression that suggests these conditions might induce further bone regeneration as well as facilitate integration of scaffolds with the surrounding host tissues. This study revealed that altering both the level of HA nanoparticle incorporation and the initial cell seeding density can effect osteoblastic differentiation and growth factor gene expression. Our results demonstrated that (1) HA addition improved surface properties of composite scaffolds by showing increased roughness, hydrophilicity, protein adsorption, and initial cell attachment, (2) up-regulation of osteogenic signal expression was also controlled by both HA amount and initial cell seeding density, and (3) subsequent osteoblastic differentiation of rat BMSCs on 3D scaffolds was facilitated by the incorporation of HA and lower cell seeding density.

Supplementary Material

Refer to Web version on PubMed Central for supplementary material.

Acknowledgments

This work was supported by the National Institute of Health (R01-DE013740) and the National Science Foundation (CBET 0448684). The authors appreciate the support of the Maryland NanoCenter and its Nanoscale Imaging, Spectroscopy, and Properties Laboratory (NISPLab). The NISPLab is supported in part by the NSF as a Materials Research Science and Engineering Center Shared Experimental Facility.

References

1. Chuenjitkuntaworn B, Inrung W, Damrongsri D, Mekaapiruk K, Supaphol P, Pavasant P. Polycaprolactone/hydroxyapatite composite scaffolds: preparation, characterization, and in vitro and in vivo biological responses of human primary bone cells. Journal of biomedical materials research 2010;94:241–51. [PubMed: 20166220]
2. Wang H, Li Y, Zuo Y, Li J, Ma S, Cheng L. Biocompatibility and osteogenesis of biomimetic nano-hydroxyapatite/polyamide composite scaffolds for bone tissue engineering. Biomaterials 2007;28:3338–48. [PubMed: 17481726]
3. Kim S, Kim SS, Lee SH, Eun Ahn S, Gwak SJ, Song JH, Kim BS, Chung HM. In vivo bone formation from human embryonic stem cell-derived osteogenic cells in poly(d,l-lactic-co-glycolic acid)/hydroxyapatite composite scaffolds. Biomaterials 2008;29:1043–53. [PubMed: 18023477]
4. Lee JH, Rim NG, Jung HS, Shin H. Control of Osteogenic Differentiation and Mineralization of Human Mesenchymal Stem Cells on Composite Nanofibers Containing Poly[lactic-co-(glycolic acid)] and Hydroxyapatite. Macromolecular bioscience. 2009
5. Ngiam M, Liao S, Patil AJ, Cheng Z, Chan CK, Ramakrishna S. The fabrication of nano-hydroxyapatite on PLGA and PLGA/collagen nanofibrous composite scaffolds and their effects in osteoblastic behavior for bone tissue engineering. Bone 2009;45:4–16. [PubMed: 19358900]
6. Niu X, Feng Q, Wang M, Guo X, Zheng Q. Porous nano-HA/collagen/PLLA scaffold containing chitosan microspheres for controlled delivery of synthetic peptide derived from BMP-2. J Control Release 2009;134:111–7. [PubMed: 19100794]
7. Lee KW, Wang S, Yaszemski MJ, Lu L. Physical properties and cellular responses to crosslinkable poly(propylene fumarate)/hydroxyapatite nanocomposites. Biomaterials 2008;29:2839–48. [PubMed: 18403013]
8. Lewandrowski KU, Bondre SP, Wise DL, Trantolo DJ. Enhanced bioactivity of a poly(propylene fumarate) bone graft substitute by augmentation with nano-hydroxyapatite. Biomed Mater Eng 2003;13:115–24. [PubMed: 12775902]
9. Heo SJ, Kim SE, Wei J, Kim DH, Hyun YT, Yun HS, Kim HK, Yoon TR, Kim SH, Park SA, Shin JW, Shin JW. In vitro and animal study of novel nano-hydroxyapatite/poly(epsilon-caprolactone) composite scaffolds fabricated by layer manufacturing process. Tissue engineering 2009;15:977–89. [PubMed: 18803480]
10. Gupta D, Venugopal J, Mitra S, Giri Dev VR, Ramakrishna S. Nanostructured biocomposite substrates by electrospinning and electrospraying for the mineralization of osteoblasts. Biomaterials 2009;30:2085–94. [PubMed: 19167752]
11. Patel M, Dunn TA, Tostanoski S, Fisher JP. Cyclic acetal hydroxyapatite composites and endogenous osteogenic gene expression of rat marrow stromal cells. Journal of tissue engineering and regenerative medicine 2010;4:422–36. [PubMed: 20047194]
12. Patel M, Patel KJ, Caccamese JF, Coletti DP, Sauk JJ, Fisher JP. Characterization of cyclic acetal hydroxyapatite nanocomposites for craniofacial tissue engineering. Journal of biomedical materials research 2010;94:408–18. [PubMed: 20186741]
13. Shi Z, Huang X, Cai Y, Tang R, Yang D. Size effect of hydroxyapatite nanoparticles on proliferation and apoptosis of osteoblast-like cells. Acta biomaterialia 2009;5:338–45. [PubMed: 18753024]
14. Kim K, Dean D, Mikos AG, Fisher JP. Effect of Initial Cell Seeding Density on Early Osteogenic Signal Expression of Rat Bone Marrow Stromal Cells Cultured on Cross-Linked Poly(propylene fumarate) Disks. Biomacromolecules. 2009
15. Cooke MN, Fisher JP, Dean D, Rimnac C, Mikos AG. Use of stereolithography to manufacture critical-sized 3D biodegradable scaffolds for bone ingrowth. J Biomed Mater Res B Appl Biomater 2003;64:65–9. [PubMed: 12516080]
16. Lee JW, Lan PX, Kim B, Lim G, Cho DW. Fabrication and characteristic analysis of a poly(propylene fumarate) scaffold using micro-stereolithography technology. J Biomed Mater Res B Appl Biomater 2008;87:1–9. [PubMed: 18335437]

17. Lee KW, Wang S, Fox BC, Ritman EL, Yaszemski MJ, Lu L. Poly(propylene fumarate) bone tissue engineering scaffold fabrication using stereolithography: effects of resin formulations and laser parameters. Biomacromolecules 2007;8:1077–84. [PubMed: 17326677]

18. Horch RA, Shahid N, Mistry AS, Timmer MD, Mikos AG, Barron AR. Nanoreinforcement of poly(propylene fumarate)-based networks with surface modified alumoxane nanoparticles for bone tissue engineering. Biomacromolecules 2004;5:1990–8. [PubMed: 15360315]

19. Mistry AS, Cheng SH, Yeh T, Christenson E, Jansen JA, Mikos AG. Fabrication and in vitro degradation of porous fumarate-based polymer/alumoxane nanocomposite scaffolds for bone tissue engineering. Journal of biomedical materials research 2009;89:68–79. [PubMed: 18428800]

20. Mistry AS, Mikos AG, Jansen JA. Degradation and biocompatibility of a poly(propylene fumarate)-based/alumoxane nanocomposite for bone tissue engineering. Journal of biomedical materials research 2007;83:940–53. [PubMed: 17580323]

21. Mistry AS, Pham QP, Schouten C, Yeh T, Christenson EM, Mikos AG, Jansen JA. In vivo bone biocompatibility and degradation of porous fumarate-based polymer/alumoxane nanocomposites for bone tissue engineering. Journal of biomedical materials research. 2009

22. Shi X, Hudson JL, Spicer PP, Tour JM, Krishnamoorti R, Mikos AG. Injectable nanocomposites of single-walled carbon nanotubes and biodegradable polymers for bone tissue engineering. Biomacromolecules 2006;7:2237–42. [PubMed: 16827593]

23. Cai ZY, Yang DA, Zhang N, Ji CG, Zhu L, Zhang T. Poly(propylene fumarate)/(calcium sulphate/beta-tricalcium phosphate) composites: preparation, characterization and in vitro degradation. Acta biomaterialia 2009;5:628–35. [PubMed: 18951071]

24. Dean D, Wolfe MS, Ahmad Y, Totonchi A, Chen JE, Fisher JP, Cooke MN, Rimnac CM, Lennon DP, Caplan AI, Topham NS, Mikos AG. Effect of transforming growth factor beta 2 on marrow-infused foam poly(propylene fumarate) tissue-engineered constructs for the repair of critical-size cranial defects in rabbits. Tissue Eng 2005;11:923–39. [PubMed: 15998232]

25. Sethuraman S, Nair LS, El-Amin S, Nguyen MT, Singh A, Greish YE, Allcock HR, Brown PW, Laurencin CT. Development and Characterization of Biodegradable Nanocomposite Injectables for Orthopaedic Applications Based on Polyphosphazenes. J Biomater Sci Polym Ed.

26. Bitar M, Brown RA, Salih V, Kidane AG, Knowles JC, Nazhat SN. Effect of cell density on osteoblastic differentiation and matrix degradation of biomimetic dense collagen scaffolds. Biomacromolecules 2008;9:129–35. [PubMed: 18095652]

27. Grayson WL, Bhumiratana S, Cannizzaro C, Chao PH, Lennon DP, Caplan AI, Vunjak-Novakovic G. Effects of initial seeding density and fluid perfusion rate on formation of tissue-engineered bone. Tissue engineering 2008;14:1809–20. [PubMed: 18620487]

28. Lode A, Bernhardt A, Gelinsky M. Cultivation of human bone marrow stromal cells on three-dimensional scaffolds of mineralized collagen: influence of seeding density on colonization, proliferation and osteogenic differentiation. Journal of tissue engineering and regenerative medicine 2008;2:400–7. [PubMed: 18756590]

29. van Gaalen SM, de Bruijn JD, Wilson CE, van Blitterswijk CA, Verbout AJ, Alblas J, Dhert WJ. Relating cell proliferation to in vivo bone formation in porous Ca/P scaffolds. Journal of biomedical materials research. 2009

30. Fisher JP, Timmer MD, Holland TA, Dean D, Engel PS, Mikos AG. Photoinitiated cross-linking of the biodegradable polyester poly(propylene fumarate). Part I. Determination of network structure. Biomacromolecules 2003;4:1327–34. [PubMed: 12959602]

31. Crowley J, Chalivendra VB. Mechanical characterization of ultra-high molecular weight polyethylene-hydroxyapatite nanocomposites. Biomed Mater Eng 2008;18:149–60. [PubMed: 18725695]

32. He J, Genetos DC, Leach JK. Osteogenesis and trophic factor secretion are influenced by the composition of hydroxyapatite/poly(lactide-co-glycolide) composite scaffolds. Tissue engineering. 2009

33. Kim SS, Sun Park M, Jeon O, Yong Choi C, Kim BS. Poly(lactide-co-glycolide)/hydroxyapatite composite scaffolds for bone tissue engineering. Biomaterials 2006;27:1399–409. [PubMed: 16169074]

34. Woo KM, Chen VJ, Ma PX. Nano-fibrous scaffolding architecture selectively enhances protein adsorption contributing to cell attachment. Journal of biomedical materials research 2003;67:531–7. [PubMed: 14566795]
35. Park H, Temenoff JS, Tabata Y, Caplan AI, Mikos AG. Injectable biodegradable hydrogel composites for rabbit marrow mesenchymal stem cell and growth factor delivery for cartilage tissue engineering. Biomaterials 2007;28:3217–27. [PubMed: 17445882]
36. Gronthos S, Simmons PJ, Graves SE, Robey PG. Integrin-mediated interactions between human bone marrow stromal precursor cells and the extracellular matrix. Bone 2001;28:174–81. [PubMed: 11182375]
37. Gajjeraman S, He G, Narayanan K, George A. Biological assemblies provide novel templates for the synthesis of hierarchical structures and facilitate cell adhesion. Advanced functional materials 2008;18:3972–80. [PubMed: 19768126]
38. Chastain SR, Kundu AK, Dhar S, Calvert JW, Putnam AJ. Adhesion of mesenchymal stem cells to polymer scaffolds occurs via distinct ECM ligands and controls their osteogenic differentiation. Journal of biomedical materials research 2006;78:73–85. [PubMed: 16602124]
39. Rouahi M, Champion E, Hardouin P, Anselme K. Quantitative kinetic analysis of gene expression during human osteoblastic adhesion on orthopaedic materials. Biomaterials 2006;27:2829–44. [PubMed: 16427124]
40. Gibson LJ. The mechanical behaviour of cancellous bone. Journal of biomechanics 1985;18:317–28. [PubMed: 4008502]
41. Liao J, Zhang L, Zuo Y, Wang H, Li J, Zou Q, Li Y. Development of nanohydroxyapatite/polycarbonate composite for bone repair. Journal of biomaterials applications 2009;24:31–45. [PubMed: 19386668]
42. Chen BQ, Sun K. Mechanical and dynamic viscoelastic properties of hydroxyapatite reinforced poly(epsilon-caprolactone). Polymer Testing 2005;24:978–82.
43. Guarino V, Causa F, Netti PA, Ciapetti G, Pagani S, Martini D, Baldini N, Ambrosio L. The role of hydroxyapatite as solid signal on performance of PCL porous scaffolds for bone tissue regeneration. J Biomed Mater Res B Appl Biomater 2008;86B:548–57. [PubMed: 18335435]
44. Khatiwala CB, Kim PD, Peyton SR, Putnam AJ. ECM compliance regulates osteogenesis by influencing MAPK signaling downstream of RhoA and ROCK. J Bone Miner Res 2009;24:886–98. [PubMed: 19113908]
45. Phimphilai M, Zhao Z, Boules H, Roca H, Franceschi RT. BMP signaling is required for RUNX2-dependent induction of the osteoblast phenotype. J Bone Miner Res 2006;21:637–46. [PubMed: 16598384]
46. Choi KY, Kim HJ, Lee MH, Kwon TG, Nah HD, Furuichi T, Komori T, Nam SH, Kim YJ, Ryoo HM. Runx2 regulates FGF2-induced Bmp2 expression during cranial bone development. Dev Dyn 2005;233:115–21. [PubMed: 15765505]
47. Franceschi RT, Xiao G. Regulation of the osteoblast-specific transcription factor, Runx2: responsiveness to multiple signal transduction pathways. J Cell Biochem 2003;88:446–54. [PubMed: 12532321]
48. Beenken A, Mohammadi M. The FGF family: biology, pathophysiology and therapy. Nat Rev Drug Discov 2009;8:235–53. [PubMed: 19247306]
49. Liu Y, Wang G, Cai Y, Ji H, Zhou G, Zhao X, Tang R, Zhang M. In vitro effects of nanophase hydroxyapatite particles on proliferation and osteogenic differentiation of bone marrow-derived mesenchymal stem cells. Journal of biomedical materials research 2009;90:1083–91. [PubMed: 18671263]
50. Fickert S, Fiedler J, Brenner RE. Identification, quantification and isolation of mesenchymal progenitor cells from osteoarthritic synovium by fluorescence automated cell sorting. Osteoarthritis Cartilage 2003;11:790–800. [PubMed: 14609532]
51. Kotobuki N, Hirose M, Machida H, Katou Y, Muraki K, Takakura Y, Ohgushi H. Viability and osteogenic potential of cryopreserved human bone marrow-derived mesenchymal cells. Tissue Eng 2005;11:663–73. [PubMed: 15998208]

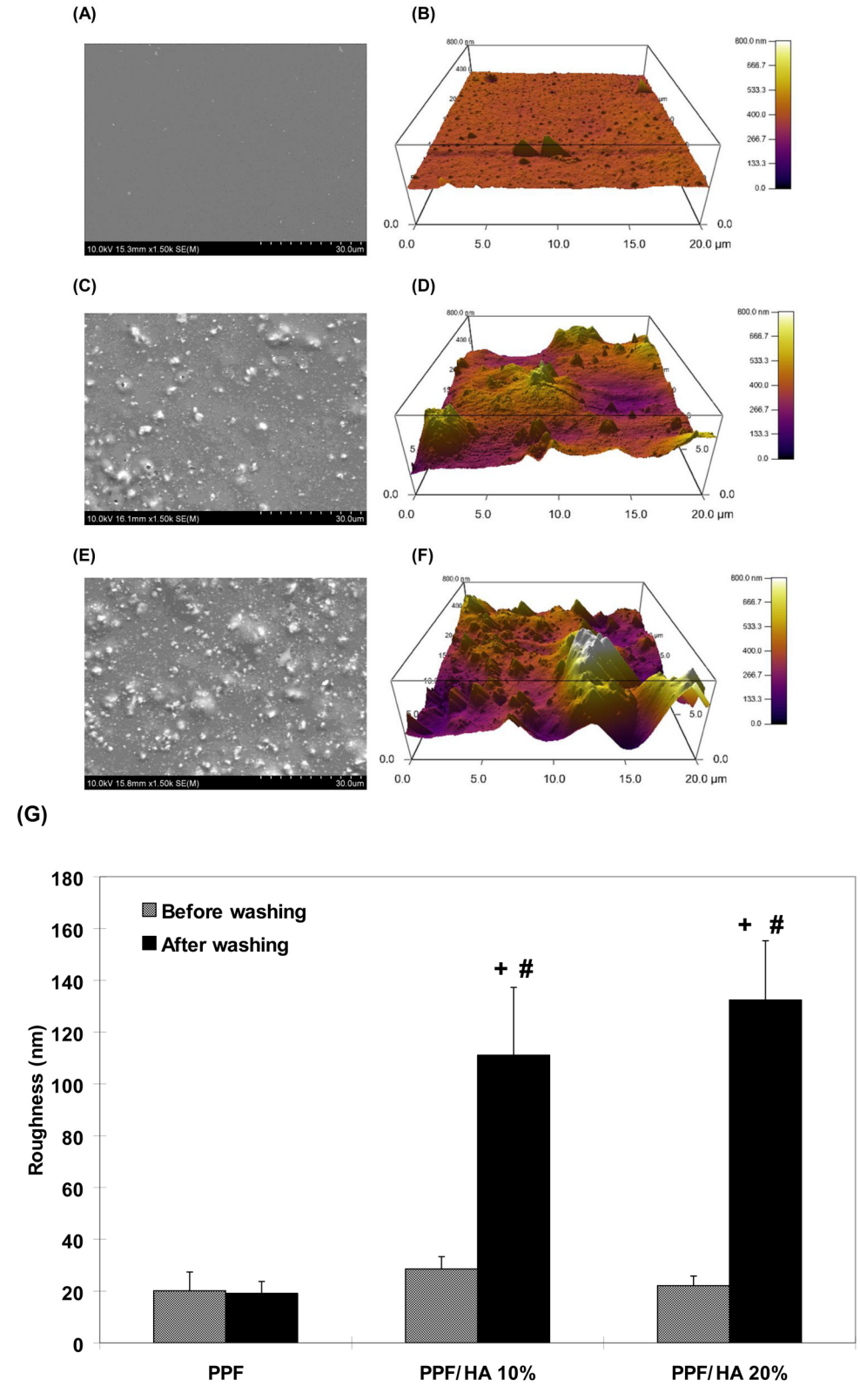

Figure 1.

Surface morphology as observed by scanning electron microscopy (SEM) images of 2D disks with PPF (A), PPF/HA10% (C), and PPF/HA20% (E). All images were obtained with 600x magnification and the scale bar represents 50 μm. These qualitative results demonstrate that HA nanoparticles were homogeneously distributed over the surface of the 2D disks and more HA content was observed with increasing HA amount. Topographic images of the surfaces by atomic force microscope (AFM) with PPF (B), PPF/HA10% (D), and PPF/HA20% (F) demonstrated that rougher surface was obtained by increasing the amount of HA. Additionally, the root mean square (RMS) roughness after the acetone washing increased significantly by adding more HA nanoparticles while the values before the acetone washing were independent of HA particle amount. + indicates a significant difference between different HA amount groups after washing ($p<0.05$), and # indicates a significant difference between before and after washing in scaffolds with the same composition ($p<0.05$) ($n=4–5$).

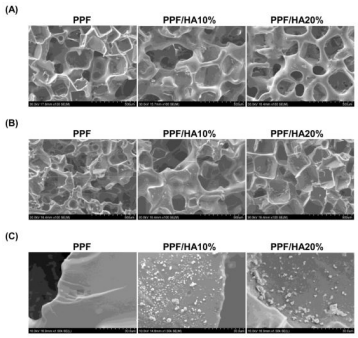

Figure 2.

SEM structural images of the top surface (A), cross sections (B), and particle distribution (C) of 3D macroporous PPF and PPF/HA scaffolds by SEM. The scale represents 500 μm in (A) and (B), and 30 μm in (C). This qualitative result demonstrates that 3D macroporous scaffolds fabricated by simple salt leaching technique showed interconnective porous structures and more HA particles were seen on the surface as the HA amount included in fabrication increased.

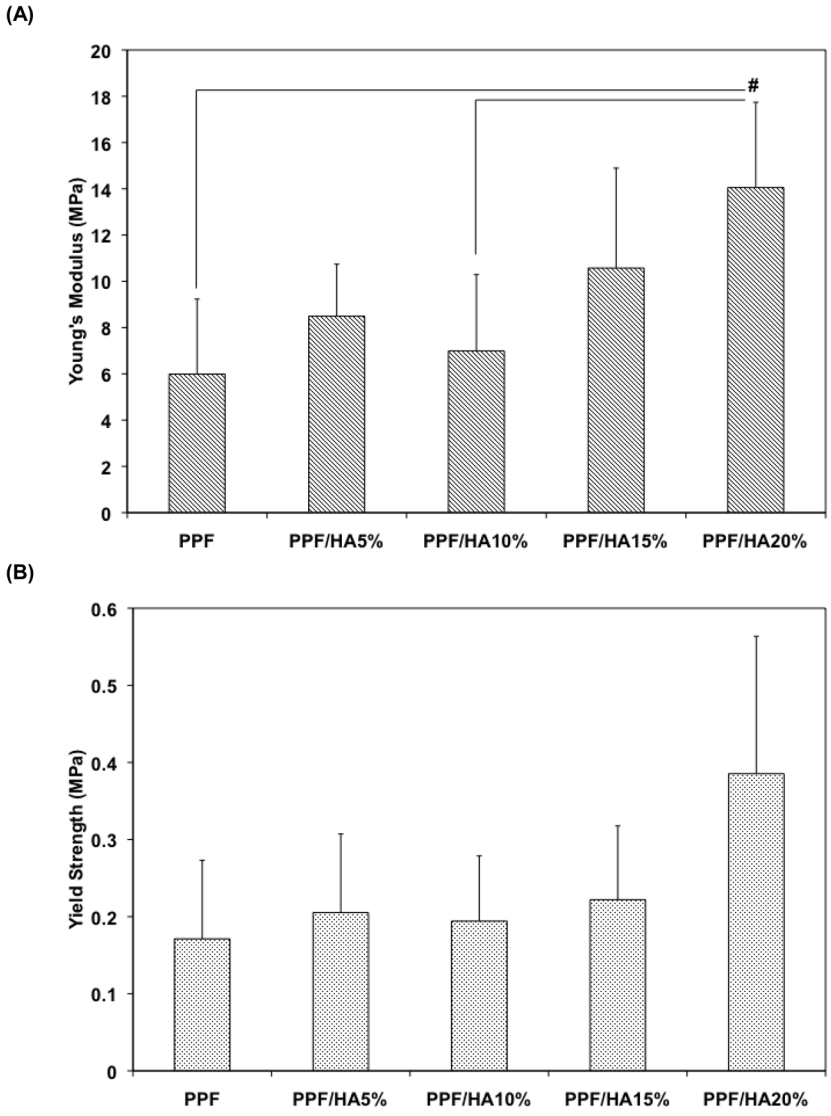

Figure 3.

Compressive properties, including Young's modulus (A) and off-set yield strength (B), of 3D macroporous PPF and PPF/HA scaffolds (n=5). The result demonstrated that the PPF/HA 20% group showed significantly higher Young's modulus than the PPF control and PPF/HA 10% groups. Off-set yield strength in the PPF/HA 20% group was also higher than in the other groups. # indicates a significant difference between groups ($p<0.05$).

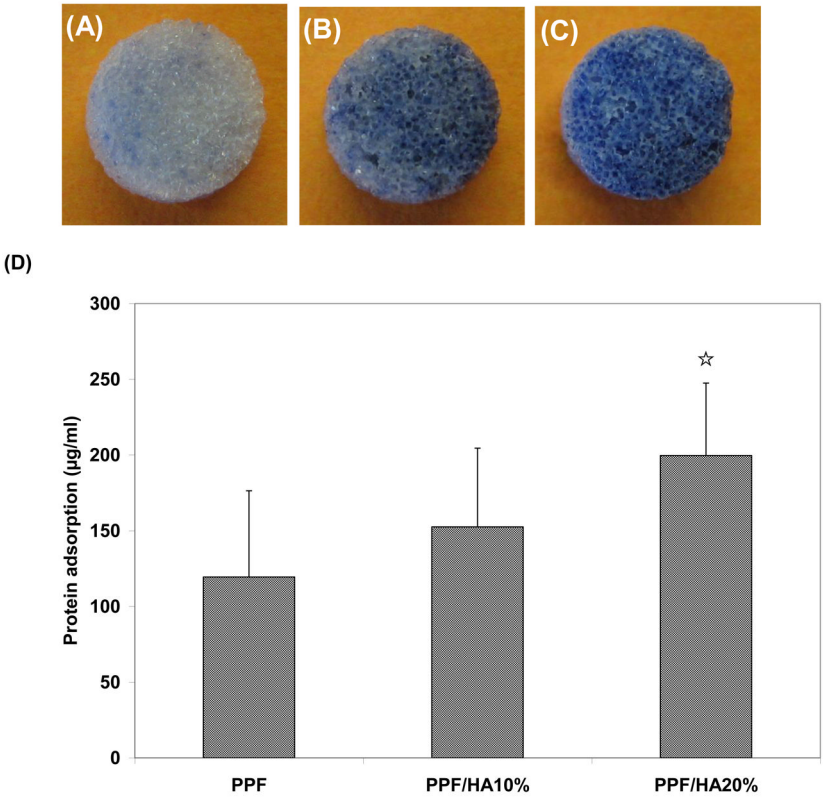

Figure 4.

HA particle distribution over the surface of scaffolds was assessed by trypan blue staining with PPF (A), PPF/HA10% (B), and PPF/HA20% (C). Protein adsorption on the PPF/HA composite scaffolds with different concentration of HA nanoparticle is shown in (D) (n=3). ☆ indicates a significant difference compared to the PPF control group ($p<0.05$).

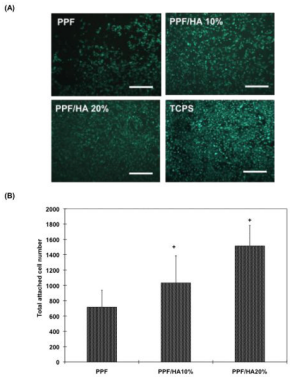

Figure 5.

Fluorescent staining images of initially attached cells on 2D disks (A) and total number of attached cell on 2D disks (B). The result in (A) qualitatively demonstrated that more viable rat BMSCs were observed in composite disks with higher amount of HA and the result in (B) verified that total attached cell number in PPF/HA 10% and 20% group were significantly higher than in the PPF control groups. Five pictures were obtained from each biological sample and biological quadruplicates were tested. + indicates a significant difference compared to PPF control group ($p<0.05$).

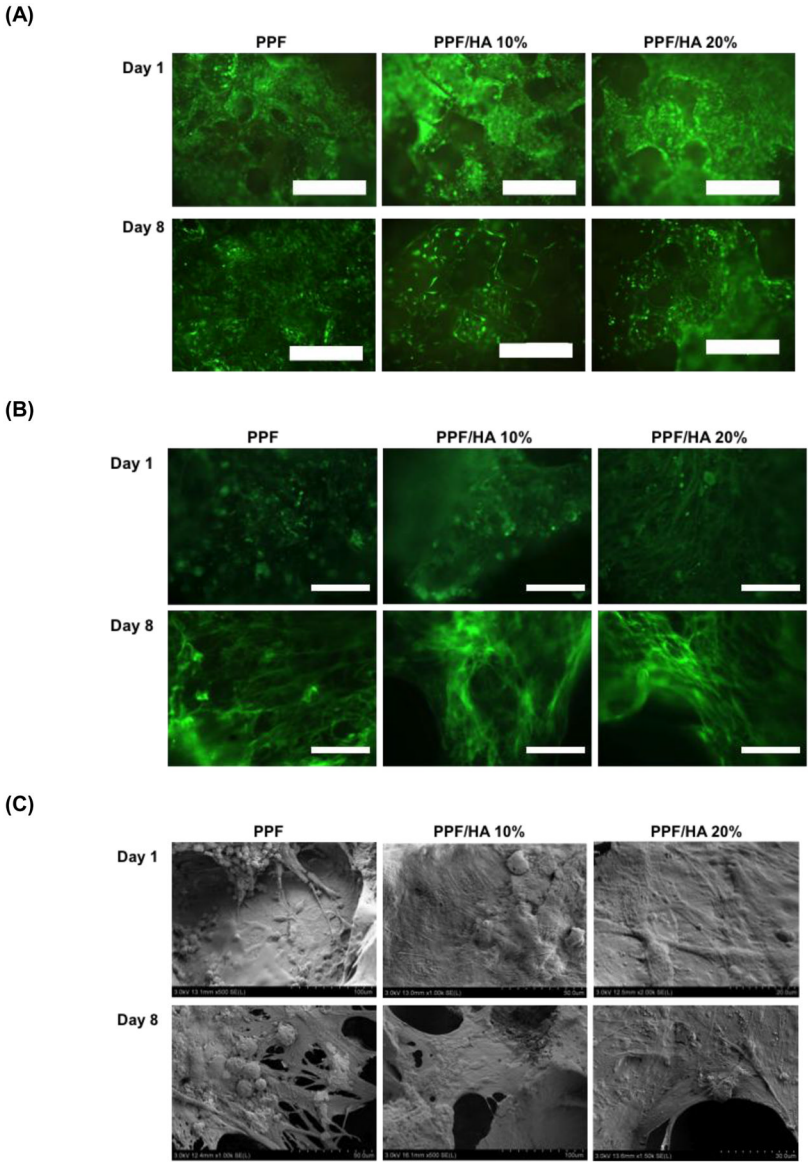

Figure 6.
Visualization of viability by Calcein AM fluorescent staining (A), F-actin staining (B), and cellular morphology by SEM (C) onto PPF composite scaffolds with different HA nanoparticle amount. The scale bar represents 300 μm in (A) and 100 μm in (B).

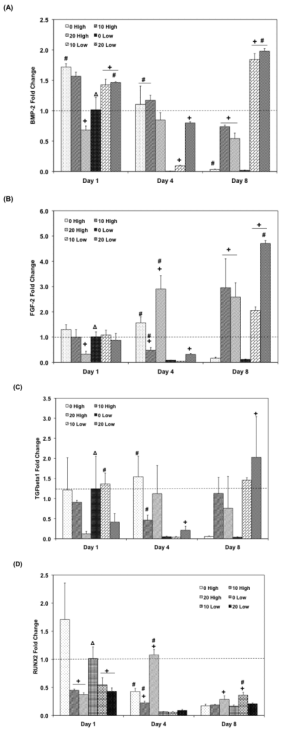

Figure 7.

Quantitative RT-PCR analysis of gene expression profiles of growth factors (A: BMP-2, B: FGF-2, C: TFG- β1, and D: Runx2) for 1, 4, and 8 days. The fold changes in gene expression level are reported as average ± standard deviation (n=3). The calibrator for all experimental groups is indicated by a Δ marker and dashed line indicates the fold change of the calibrator group. + indicates a statistical difference in HA amount within the same cell seeding density group as compared to the 0% HA control group while # indicates a statistical difference in cell seeding density groups within the same HA concentration group ($p<0.05$).

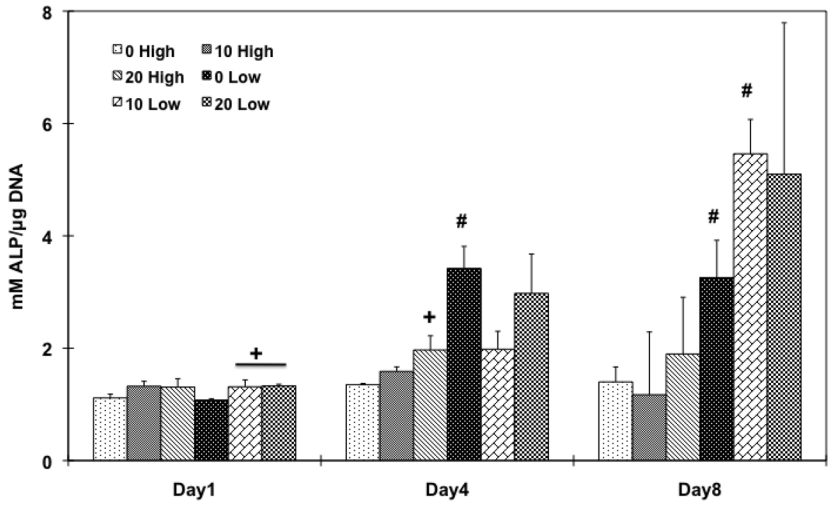

Figure 8.

ALP protein activity of rat BMSCs on PPF composite scaffolds with different HA contents and cell seeding densities for 1, 4, and 8 days. ALP protein expression level was normalized by DNA amount and average ± standard deviation (n=3 per group) is reported. + indicates a statistical difference in HA amount within the same cell seeding density group while # indicates a statistical difference in cell seeding density groups with the same HA concentration group ($p<0.05$).

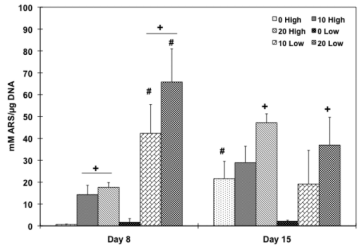

Figure 9.
Quantitative mineralization assay by alizarin red S staining on day 8 and 15. Calcium deposition level was normalized by DNA amount and average ± standard deviation (n=3 per group) is reported. + indicates a statistical difference in HA amount within same cell seeding density group while # indicates a statistical difference in cell seeding density groups with the same HA concentration group ($p<0.05$).

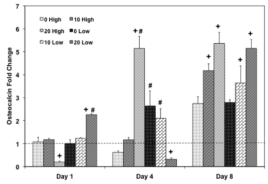

Figure 10.

Quantitative RT-PCR analysis of gene expression profiles of OC osteogenic differentiation markers for 1, 4, and 8 days. The fold changes in gene expression level are reported as average ± standard deviation (n=3). The calibrator for all experimental groups is indicated by a Δ marker and dashed line indicates the fold change of the calibrator group. + indicates a statistical difference in HA amount within the same cell seeding density group as compared to the 0% HA control group while # indicates a statistical difference in cell seeding density groups within the same HA concentration group ($p<0.05$).

Table 1

Experimental groups for 3D in vitro culture.

Groups	PPF Content (wt%)	HA Content (wt%)	Porosity (wt%)	Porosity (vol%)	Cell Density (cells/scaffold)
0 High	100%	-	75.83 ± 0.80%	64.32 ± 0.35	
10 High	90%	10%	76.54 ± 0.35%	69.21 ± 0.34	1.00×10^6
20 High	80%	20%	76.25 ± 1.10%	72.08 ± 0.80	
0 Low	100%	-	75.83 ± 0.80%	64.32 ± 0.35	
10 Low	90%	10%	76.54 ± 0.35%	69.21 ± 0.34	0.33×10^6
20 Low	80%	20%	76.25 ± 1.10%	72.08 ± 0.80	

Table 2

Percentage of elemental carbon (C), oxygen (O), calcium (Ca), and phosphate (P) on the nanocomposite surface as determined by EDS spectrum analysis (point of interest) (n=3–4).

	Element Percentages from EDS Spectrum Analysis				
Composition	**Carbon (C)**	**Oxygen (O)**	**Calcium (Ca)**	**Phosphate (P)**	**Ca/P ratio**
PPF	63.20 ± 0.30	36.53 ± 0.16	0.25 ± 0.07	-	-
PPF/HA 10%	26.13 ± 5.06	50.10 ± 4.63	15.63 ±1.60	8.15 ± 0.47	1.92 ± 0.21
PPF/HA 20%	26.54 ± 3.60	41.76 ± 7.04	21.03 ± 6.49	10.68 ± 3.74	1.99 ± 0.12